The Society for engineering in agricultural, food, and biological systems

The Canadian Society for Engineering in Agricultural, Food, and Biological Systems

An ASAE/CSAE Meeting Presentation *Paper Number: 04xxxx*

SIMULATIONS OF DISTRIBUTED WATERSHED EROSION, DEPOSITION, AND TERRAIN EVOLUTION USING A PATH SAMPLING MONTE CARLO METHOD

Christopher S. Thaxton, Ph.D.

Appalachian State University, Boone, NC, thaxtoncs@appstate.edu

Helena Mitasova, Ph.D.

North Carolina State University, Raleigh, NC, hmitaso@unity.ncsu.edu

Lubos Mitas, Ph.D.

North Carolina State University, Raleigh, NC, lubos_mitas@ncsu.edu

Rich McLaughlin, Ph.D.

North Carolina State University, Raleigh, NC, rich_mclaughlin@ncsu.edu

Written for presentation at the
2004 ASAE/CSAE Annual International Meeting
Sponsored by ASAE/CSAE
Fairmont Chateau Laurier, The Westin, Government Centre
Ottawa, Ontario, Canada
1 - 4 August 2004

Abstract. *We present a new GRASS GIS module r.terradyn that evolves a given terrain using sediment flux information provided by the SIMWE (SImulated Water Erosion) GRASS GIS modules r.sim.water and r.sim.sediment originally developed by Mitas and Mitasova (1998). SIMWE is a distributed, bivariate, steady-state watershed scale sediment erosion, transport, and deposition model that employs a path sampling Monte Carlo method in which erosion, transport, and deposition conditions are treated as a continuous field, resulting in fully distributed erosion/deposition patterns.. Module r.terradyn modifies the original digital elevation model (DEM) over time steps, each corresponding to a single rainfall event, which is then used as the input DEM for subsequent SIMWE*

and r.terradyn iterations. New techniques were derived that include the application of a gravitational diffusion term, an approximate Neumann boundary condition routine for use with GRASS GIS module r.slope.aspect, a comparative band-pass filter for numerical stability of the iterative feedback system, and a simple rainfall excess calculation methodology derived from accumulated runoff curve number tables that enables spatially distributed infiltration. Application of r.terradyn to a sample watershed demonstrates results for distributed land cover and infiltration and for various soil types. Terrain change impact from disturbed areas is also presented. Preliminary comparisons to field observations and total discharge data are currently being used to calibrate model parameters. Verification of the model is still ongoing as data becomes available. The influence of grain size dependent transport mechanisms on short-term and long-term topological changes induced by human impact, such as mining and construction, may lead to the determination of the optimum location, size, and frequency of control measures to more cost effectively meet emerging TMDL requirements.

Keywords. Sediment, detention, watershed, hydrodynamics, baffles, settling.

(The ASAE/CSAE disclaimer is on a footer on this page, and will show in Print Preview or Page Layout view.)

Introduction

Advancements in geospatial technologies have stimulated development of a wide range of tools for evaluating and managing soil erosion within watersheds (see e.g. references in Borah and Bera, 2003). Important gains in the control of soil erosion have been made; however, there remain significant problems with sedimentation of streams and water supply systems, transport of soil attached contaminants, and the cost of some management techniques, especially for severely disturbed areas or large events. While substantial knowledge has been gained for individual sediment control methods as well as for spatially averaged effects of watershed management strategies, the capability of accurately predicting the interaction between erosion processes and management methods within complex landscapes is still rather limited.

Determining the most effective locations for the design and implementation of conservation practices (e.g. selecting projects that save the most soil or benefit the most acres per dollar cost) requires detailed spatial representation (1-10m resolution) of the given area as well as models that are capable of simulating the effects of spatially and temporally variable conditions on sediment transport. While several of the existing modeling tools support spatially and temporally variable landcover and rainfall, change of topography due to erosion and sedimentation processes is usually neglected. Predictions of changes in elevation surface due to erosion and deposition have been the focus of research in geomorphology (Willgoose et al. 1991, Tucker et al. 2001) with terrain evolution simulated over long periods (hundreds of years) and spatial resolutions lower than what is needed for sediment control planning. Short term elevation changes have been the focus of research at higher resolutions, for example for the modeling of rills (Favis-Mortlock et al. 1998). Changes in elevations can be an important component of the functionality of some erosion prevention measures, such as hedges (Dabney et al. 1999) but they can also negatively impact sediment control measures by filling the sedimentation ponds and check dams and by diverting flow. High resolution digital elevation models (1-5m) that are now becoming common even for larger watersheds (e.g. North Carolina Flood Mapping Program http://www.ncfloodmaps.com/) and increases in computational power provide opportunities to incorporate terrain change into modeling of complex combinations of conservation and sediment control measures at a watershed level. In this paper, a new GIS module is presented that simulates terrain change for a sequence of events based on the hydrologic and sediment transport models described by Mitas and Mitasova (1998).

SIMWE (SImulated Water Erosion) Model

In GRASS GIS, the modules *r.sim.water* and *r.sim.sediment* are the implementation of the sediment erosion/deposition model referred to as SIMWE (SIMulated Water Erosion) developed by Mitas & Mitasova (1998). The governing continuity equation is solved via a path sampling Monte Carlo method in which erosion, transport, and deposition conditions are treated as a continuous field, resulting in fully distributed erosion/deposition patterns. In *r.sim.water*, shallow water is modeled via the two-dimensional form of the Saint Venant equations with the kinematic wave approximation $\mathbf{s}_f \approx \mathbf{s}_o$ (friction slope ≈ elevation gradient). Unit discharge [m^2/s] is:

$$\vec{q}(\vec{r},t) = \vec{v}(\vec{r},t)h(\vec{r},t) \qquad (1)$$

where ***v(r,t)*** [m/s] is the flow velocity and *h(**r**,t)* [m] is the water depth. Note that spatial variability is explicit through the governing equations for SIMWE. Manning's relation closes the system of equations. To approximate the diffusive wave effects, steady state is assumed and a

diffusion term is incorporated into the continuity equation, such that the final form of continuity for *r.sim.water* is:

$$-\frac{\varepsilon}{2}\nabla^2\left[h^{5/3}(\vec{r})\right]+\vec{\nabla}\cdot\left[h(\vec{r})\vec{v}(\vec{r})\right]=i_e(\vec{r}) \tag{2}$$

where $i_e(\boldsymbol{r})$ [m/s] is the rainfall excess. In *r.sim.sediment*, the continuity of sediment mass equation is simplified by assuming steady state:

$$\begin{aligned}&\frac{\partial\left[\rho_s c(\vec{r},t)h(\vec{r},t)\right]}{\partial t}+\vec{\nabla}\cdot\vec{q}_s(\vec{r},t)=\text{sources - sinks}=D_F(\vec{r},t)\\&\frac{\partial\left[\rho_s c(\vec{r},t)h(\vec{r},t)\right]}{\partial t}=0\ \rightarrow\ \vec{\nabla}\cdot\vec{q}_s(\vec{r})=D_F(\vec{r})\end{aligned} \tag{3}$$

where the detachment/deposition rate D_F [kg/m^2/s] is assumed to be proportional to the difference between the transport capacity, $T_C(\boldsymbol{r})$ [kg/m/s], and the sediment load, $\boldsymbol{q}_s(\boldsymbol{r})$ [kg/m/s]:

$$D_F(\vec{r})=\sigma(\vec{r})\left(T_C(\vec{r})-\left|\vec{q}_s(\vec{r})\right|\right). \tag{4}$$

The first order reaction term, $\sigma(\boldsymbol{r})$, is dependent on soil and cover properties. Here, the sediment flow rate (sediment load) is proportional to and in phase with the water flow rate (steady state):

$$\vec{q}_s(\vec{r})=\rho_s c(\vec{r})\vec{q}(\vec{r}) \tag{5}$$

where ρ_s is the density of the sediment [kg/particle], $c(\boldsymbol{r})$ is the sediment concentration [particles/m^3], and $\boldsymbol{q}(\boldsymbol{r})$ [m^2/s] is the water unit flow discharge. The final form of the sediment continuity equation is:

$$-\frac{\omega}{2}\nabla^2\wp(\vec{r})+\vec{\nabla}\cdot\left[\wp(\vec{r})\vec{v}(\vec{r})\right]+\wp(\vec{r})\sigma(\vec{r})\left|\vec{v}(\vec{r})\right|=\sigma(\vec{r})T(\vec{r}) \tag{6}$$

where

$$\wp(\vec{r})=\rho_s c(\vec{r})h(\vec{r})\quad[\text{kg/m}^3] \tag{7}$$

Similar to WEPP (Foster, 1989), SIMWE defines transport capacity as:

$$T_C(\vec{r})=K_t(\vec{r})\tau(\vec{r})_f^p \tag{8}$$

and the detachment capacity, $D_C(\boldsymbol{r})$ [kg/m^2/s], as:

$$D_C(\vec{r})=K_d(\vec{r})\left(\tau_f(\vec{r})-\tau_c(\vec{r})\right)^q\quad;\quad q=1 \tag{9}$$

Here, $K_t(\boldsymbol{r})$ is the transport capacity coefficient and $K_d(\boldsymbol{r})$ is the maximum detachment coefficient. The first order reaction term is therefore defined as $\sigma(\boldsymbol{r})=D_c(\boldsymbol{r})/T(\boldsymbol{r})$. If $p=q=1$, and critical shear is neglected (suggested by Foster, 1982, who states that the presence of a critical shear will underestimate sediment load), $\sigma(\boldsymbol{r})$ equates to $K_d(\boldsymbol{r})/K_t(\boldsymbol{r})$. The flow shear stress, τ_f [Pa], is defined at every location in the watershed as simply:

$$\tau_f=\rho_W g h(\vec{r})\sin\beta(\vec{r}) \tag{10}$$

Here, $\rho_w g=\gamma$ [kg/m^2/s^2] is the specific gravity of water, $h(\boldsymbol{r})=R$ [m] is the hydraulic radius, and $\sin(\beta)$ is the bed slope (gentle slopes assumed).

In the case for which $T_C \le q_S$ (transport-limited):

$$\frac{D_F(\vec{r})}{D_C(\vec{r})}+\frac{|\vec{q}_s(\vec{r})|}{T_C(\vec{r})}=1;\qquad \frac{|\vec{q}_s(\vec{r})|}{T_C(\vec{r})}\approx 1. \tag{11}$$

The transport limited case can be described as $\sigma \rightarrow \infty$ ($K_t(\mathbf{r}) \leq K_d(\mathbf{r})$); however, although this condition is satisfied with a dominant $K_d(\mathbf{r})$, detachment limited erosion may occur as long as the sediment load is less than the transport capacity. Mitas and Mitasova (1998) apply the continuity condition and solve for $D_F(\mathbf{r})$ in terms of profile curvature, κ_p, and tangential curvature, κ_t. In their resulting bivariate solution,

$$D_F(\vec{r})=\vec{\nabla}\cdot|\vec{q}_s|\hat{s}_0=\vec{\nabla}\cdot T_C(\vec{r})\hat{s}_0=K_t(\vec{r})\rho_W g\left\{\vec{\nabla}h(\vec{r})\cdot\hat{s}_0\sin\beta-h(\vec{r})\left[\kappa_p+\kappa_t\right]\right\} \tag{12}$$

the local flow acceleration in both the gradient and tangential directions play equally important roles in the spatial distribution of erosion and deposition (see Mitas and Mitasova, 1998, Appendix). Here, β is the slope angle, $\mathbf{s_o}$ is the unit vector in the steepest slope direction, and h [m] is the depth of overland flow. This process includes soil properties via $K_t(\mathbf{r})$ and is superior when compared to conventional univariate formalisms which underpredict deposition in areas of tangential concavity. Unlike WEPP, however, which employs grain size dependence via settling velocity in their deposition condition, grain size dependence is limited to the first order reaction term, σ, and critical shear, τ_C.

In the case of $T_C >> q_S$ (detachment-limited),

$$\frac{D_F(\vec{r})}{D_C(\vec{r})}+\frac{|\vec{q}_s(\vec{r})|}{T_C(\vec{r})}=1;\qquad \frac{|\vec{q}_s(\vec{r})|}{T_C(\vec{r})}\approx 0\ \rightarrow\ D_F(\vec{r})=D_C(\vec{r}) \tag{13}$$

and detachment is dictated by equation (9). The detachment limited case can be described as $\sigma \rightarrow 0$ ($K_d(\mathbf{r}) << K_t(\mathbf{r})$). Although this condition is satisfied with a dominant $K_t(\mathbf{r})$, transport limited erosion will occur as long as the sediment load is close to the transport capacity. Care should be taken when using relative values of $K_d(\mathbf{r})$ and $K_t(\mathbf{r})$ as inputs to SIMWE in forcing detachment or transport limited conditions within the model.

Terrain Evolution

The terrain evolution equation used in this treatment is (e.g. Willgoose et al., 1991; Lei et al., 1997):

$$\frac{\partial z(\vec{r},t)}{\partial t}=-\frac{1}{\rho_b(\vec{r})}\vec{\nabla}\cdot\left(q_s(\vec{r},t)\hat{s}_0(\vec{r},t)-\varepsilon_g(\vec{r})\nabla z(\vec{r},t)\right) \tag{14}$$

where $D_b(\mathbf{r})$ [kg/m^3] is the bulk density of the sediment

$$\rho_b(\vec{r})=\rho_s(1-\lambda(\vec{r})) \tag{15}$$

Here, ρ_s [kg/m^3] is the density of the sediment and $\lambda(\mathbf{r})$ [dimensionless] is the bed porosity. The diffusion coefficient, $\varepsilon_g(\mathbf{r})$ [m^2/s], and the bulk density can vary spatially depending on the soil type; however, in our current implementation we assumed that $\varepsilon_g(\mathbf{r})=\varepsilon_g$ and $D_b(\mathbf{r})=D_b$ are constants. Equation (14) without the diffusion term is the basic sediment conservation equation (a.k.a. the Exner equation) commonly used in terrain change models (Tucker et al., 2001; Parker et al., 2000; Dietrich et al., 1993; Karrambas and Koutitas, 2002). The second term in equation (14) is a gravitational diffusion term which takes into account the effects of local curvature. Physically, the diffusion term represents the localized migration and settling of soil that occurs during and between rainfall events. It is similar in nature to the diffusive hillslope

erosion term used by Tucker and Bras (1998), except that in this case, diffusion is not forced based on a landslide stability threshold but rather is a correction that is proportional to the continuous slope.

Implementation via GRASS GIS module r.terradyn

To implement the terrain evolution equation within *r.terradyn*, equation (14) is solved via a two-stage time stepping routine. First, the elevation change due to the erosion/deposition rates is computed via the boundary value equation at time step t+½:

$$z\left(\vec{r},t+\tfrac{1}{2}\right)=z\left(\vec{r},t\right)-\frac{\Delta t}{2}\frac{1}{\rho_b}\vec{\nabla}\cdot\left[q_s\left(\vec{r},t\right)\hat{s}_0\left(\vec{r},t\right)\right] \tag{16}$$

A mass-conservative band-pass filter (Thaxton, 2004) is applied to the elevation change histogram (the second term in equation (16)) prior to solving for $z(r)^{t+½}$. The final elevation change is then computed at time *t* based on the elevation at time *t+½*:

$$z\left(\vec{r},t+1\right)=z\left(\vec{r},t+\tfrac{1}{2}\right)+\frac{\Delta t}{2}\frac{\varepsilon_g}{\rho_b}\nabla^2 z\left(\vec{r},t+\tfrac{1}{2}\right) \tag{17}$$

This is a diffusive (parabolic) PDE which is subject to numerical stability constraints (see Thaxton, 2004). The user has the option of smoothing the resulting terrain change locally to remove small scale fluctuations on the order of *)x*. The flowchart for *r.terradyn* is illustrated in figure 1. This is a feedback network, susceptible to rapidly divergent behavior due to signal amplification. The band-pass filter and the smoothing algorithm are intended to attenuate numerical instability of the feedback system that emerges in the form of localized regions of exponential terrain change. The gravitational diffusion term assists in this process inherently, although it is intended to model the actual physical behavior of the soil that migrates and settles during and between rainfall events.

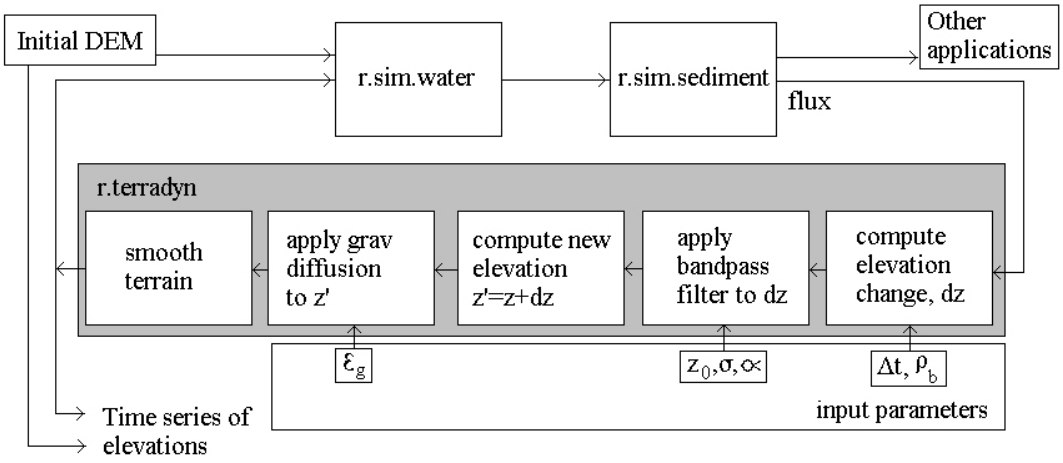

Figure 1: Flowchart of *r.terradyn* module.

Numerical implementation of *r.terradyn* is done within GRASS GIS as a UNIX shell script. To compute the terrain at time *t+1*, *r.terradyn* requires the DEM (digital elevation model) at time *t*, the slope and aspect angles of the DEM, the sediment load as output from *r.sim.sediment*, as well as control parameters which include the bulk density, the time step size, the gravitational

diffusion coefficient, and control values for the smoothing and band-pass filter algorithms. The initial DEM is obtained from existing data (available, for example, via USGS National Elevation Data (NED) data set), ground field surveys, or LIDAR (Light Detection And Ranging) airborne surveys (see Neteler and Mitasova, 2002). Once the DEM is in raster form, the slope and aspect are determined using GRASS GIS module *r.slope.aspect* (with a modified Neumann boundary condition, see Thaxton, 2004) which employs the definitions of slope and aspect described in Neteler and Mitasova (2002). The smoothing routine uses GRASS GIS module *r.neighbors method=average size=X* (where *X* is user defined. *X* is odd and can range from 1 to 25).

Application to the Lake Wheeler Road watershed

The Lake Wheeler Road farm complex at North Carolina State University was used as an experimental watershed for development and verification of *r.terradyn*. The facility is comprised mostly of open fields and row crops, with thin woods scattered throughout, as well as roads and buildings at various locations (figure 2). The DEM was obtained from field surveys at 2m x 2m (x-y grid) resolution. Simulations were performed on a sub-watershed (boxed region in figure 2) of roughly 200 x 200 grid cells in size (~33 acres). The southeast corner of the study region is bounded by roads which are elevated ~1.5m relative to the watershed DEM in that area. GRASS GIS 5.03 and 5.3 versions were run on Linux workstations running Redhat™ 9.0. The 3-D images were generated via GRASS GIS module *nviz* with an elevation exaggeration of 3.0 to 4.0.

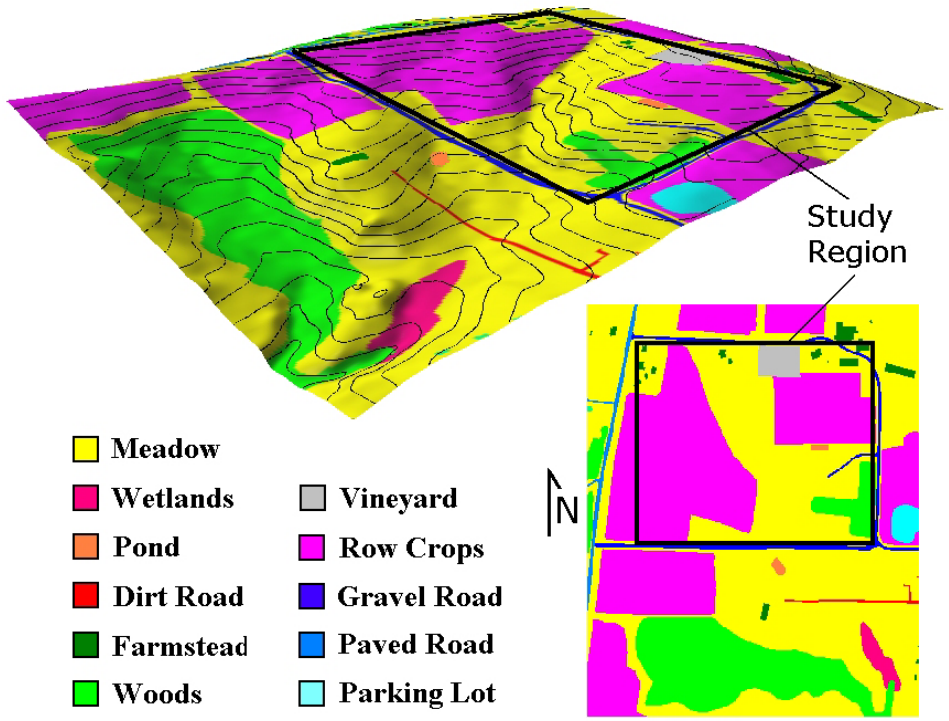

Figure 2: The Lake Wheeler Road farm watershed at NC State University. Land cover is indicated by the color key. Simulations were performed on the sub-region indicated by the box.

The *r.terradyn* module called *r.sim.water* and *r.sim.sediment* with *niter=1000* (the number of SIMWE iterations) and *nwalkers=1000000* (the number of SIMWE walkers), *diffc=0.3* (the SIMWE water diffusion coefficient) and *halpha=10* (the SIMWE diffusion correction term). The

number of walkers used in these simulations produced the accuracy necessary for terrain evolution at the chosen grid resolution and the number of iterations allowed for water flow and sediment flux equilibrium. The band pass filter parameters were such that the maximum allowable elevation change (10 mm) per iteration would not noticeably affect the long term net terrain evolution results within the parameter spaces simulated. The gravitational diffusion term, ε_g, was set to 0.2 - this value was chosen based on stability criterion (Thaxton, 2004) and was observed to produce results that most accurately modeled expected terrain change. The duration of each rainfall event was set to Δt=60 minutes, the sediment density 2650 kg/m^3, and the porosity was λ=0.5 such that $\Delta t/\rho_b$=2.7 [m^{3}s/kg]. Simulations were run out to 30 iterations (~2 years). Randomized rainfall about a mean of 1.0E-5 m/s was employed for all simulations (Thaxton, 2004) unless otherwise noted - rainfall logs are shown as a time series imbedded in the elevation DEM results from each run where applicable.

Photographs were taken of the Lake Wheeler Road farm just following a rainfall event of 1.07 inches/hour on July 29, 2003 as recorded by the State Climate Office of North Carolina (http://www.nc-climate.ncsu.edu), at the location indicated (figure 3). The water that was confined to channel flow was approximately 0.3m deep in agreement with predicted steady state water depths from *r.terradyn*.

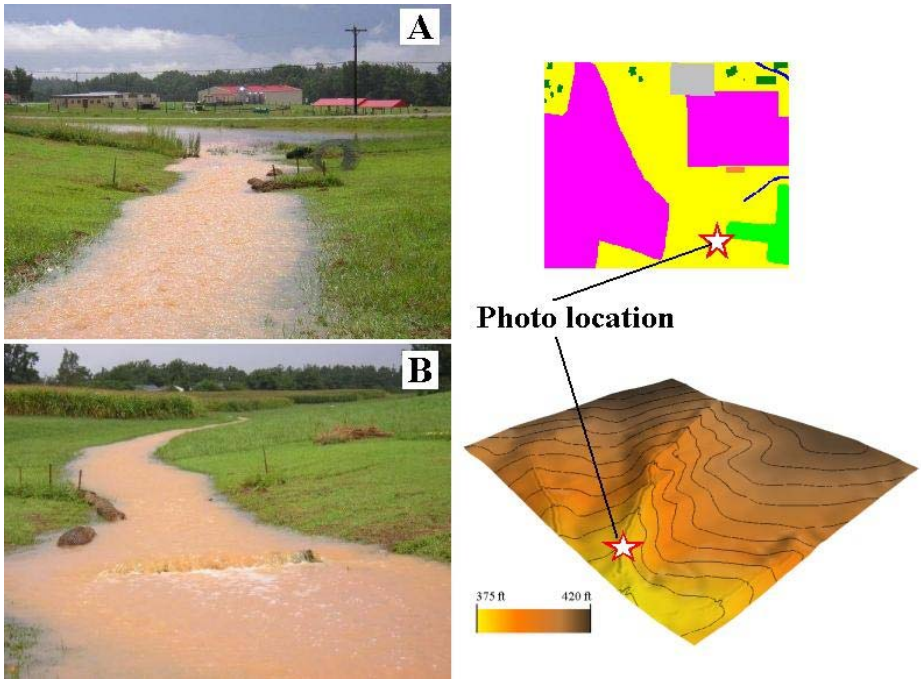

Figure 3: Photographs of the study region during a rain event. Photos were taken at the location in the study region indicated by the star in the topographical reference maps. Perspectives are (A) downhill toward the region of net sediment deposition and (B) uphill toward the channel incision.

A set of simulations was performed with CNII-D (curve number - soil type, see Haan, et al. 1994) distributed infiltration conditions and distributed model input parameters, Manning's n, K_d, K_t, and τ_c , as defined in table 1 (see: http://skagit.meas.ncsu.edu/~helena). The results are summarized in figure 4 in which the colors representing net elevation change are overlaid upon the DEM after 30 iterations of *r.terradyn*. Also included are the (A) water depth [m], (B) sediment flux [kg/m/s], (C) flow discharge [m^3/s], and (D) erosion / deposition pattern (smoothed) [kg/m^2/s] from r.sim.sediment (not used by r.terradyn) at iteration #29, in which the rainfall was 1.3E-5 m/s. Note that the woods in the south-east corner of the sub-region (bottom-

right of image) accrued significant sediment due to the imposed reduction in transport capacity of the land cover (which was magnified in runs with higher rainfall rates - not shown). This effect has been observed in the field and illustrates the potential for damaging sediment accumulation (and elevation increase) in vegetal zones designed for sedimentation control.

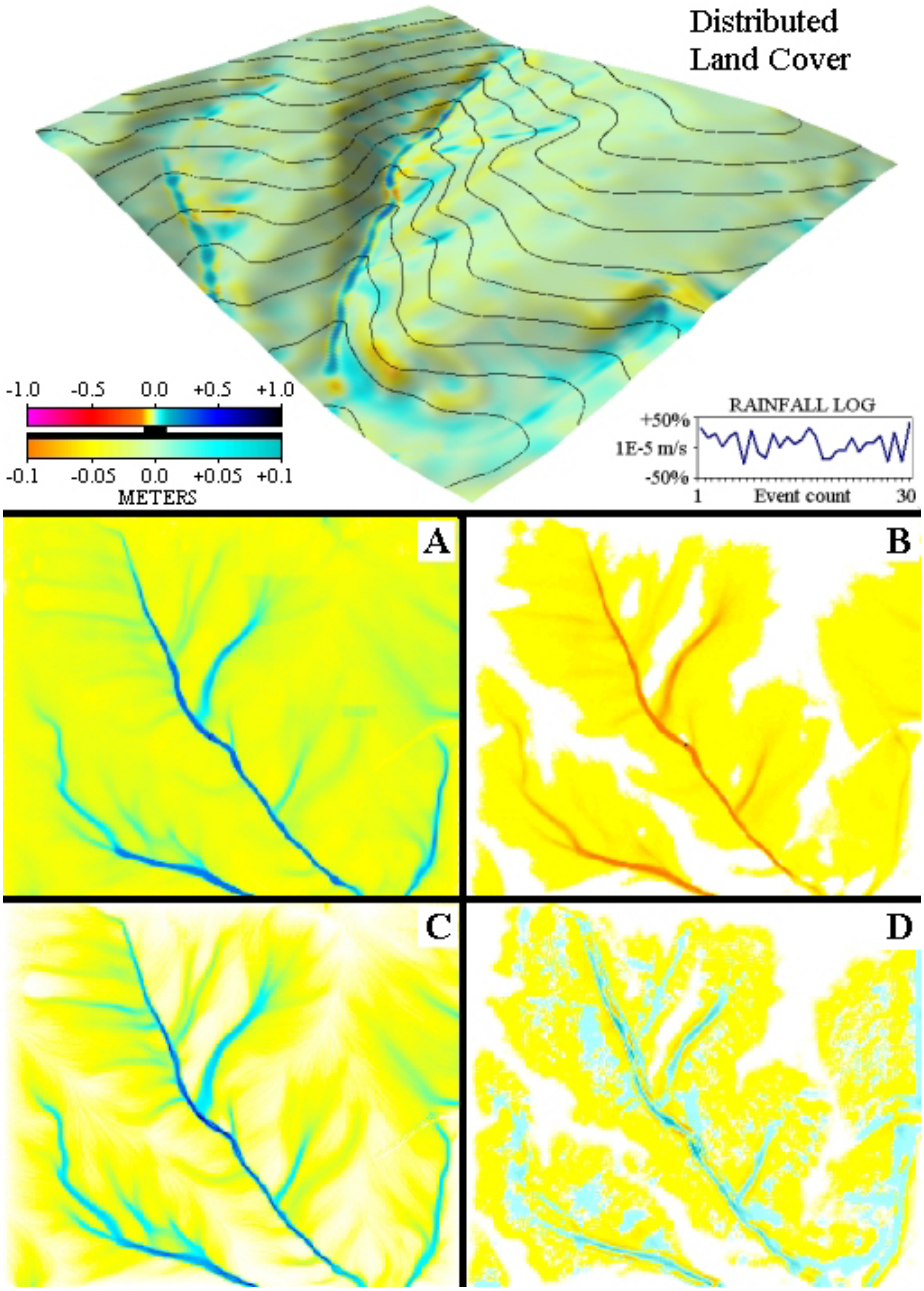

Figure 4: The modified DEM of the Lake Wheeler sub-watershed after 30 r.terradyn iterations with distributed land cover per table 1 with CNII-D distributed infiltration. Also included are the (A) water depth [m], (B) sediment flux [kg/m/s], (C) flow discharge [m^3/s], and (D) erosion / deposition pattern (smoothed) [$kg/m^2/s$] from r.sim.sediment (not used by r.terradyn) at iteration #29, in which the rainfall was 1.3E-5 m/s.

Table 1: Cover and soil parameters used in the distributed simulations.

Land cover	Manning's n	K_t	K_d	τ_c	CNII-D
Pond	0.99	1.0000	0.000000	7.00	98
Woods	0.40	0.0001	0.000271	2.03	83†
Homestead	0.03	0.0008	0.000300	7.00	86
Parking lot	0.03	0.0008	0.000300	2.40	98
Paved road	0.01	1.0000	0.000000	7.00	93
Gravel road	0.03	0.0008	0.000300	2.40	91
Vineyard	0.06	0.0010	0.000607	1.00	94
Row crops	0.17	0.0005	0.000450	2.03	91†
Wetlands	0.99	1.0000	0.000000	7.00	98
Dirt road	0.03	0.0008	0.000300	2.40	89
Meadow	0.24	0.0005	0.000367	2.03	78

† Poor cover conditions: Woods- litter, small brush and trees destroyed by heavy grazing or regular burning; Row crops- without conservation treatments.

To simulate the behavior of different soil types within *r.terradyn*, a baseline run was performed with static land cover (K_t,=K_d=0.001, Manning's n=0.05, and τ_c=0.01) and zero infiltration as well as a set of runs in which K_t, K_d, and τ_c were varied per table 2. Figure 5 shows the DEMs, overlaid by the colors representing net elevation change after 30 iterations of *r.terradyn*, for the baseline and for each of the soil types in table 2. For silt and larger grain sizes, a marked reduction in erosion and deposition was obtained as compared to the runs in which K_t was fixed to 0.01 (not shown). The maximum net elevation changed occurred for the silt sized grains.

Table 2: Grain size specific parameters chosen for the soil types simulated. Typical sediment characteristics for Midwestern soil taken from Young, et. al. (1978) and Foster (1982). Also used by AnnAGNPS

Soil type	K_t	K_d	$\sigma=D_c/T_c$	Critical Shear	Specific Gravity	Size [microns]	V_f [mm/s]
Clay	0.1000	0.00089	0.0089	0.01	2.65	2	0.00311
Silt	0.0200	0.00148	0.0740	0.05	2.65	10	0.0799
Sand	0.0050	0.00155	0.3100	0.10	2.65	20	0.0381
Small Aggregates	0.0005	0.01100	22.000	0.80	1.80	200	23.1
Large Aggregates	0.0004	0.01280	32.000	1.00	1.80	500	34.7

Results from a disturbed watershed

A final set of simulations was performed to model the effects of disturbance by removing the land cover at selected locations within the study region. The region was assumed to have the same distributed land cover as in table 1 but with the previously identified areas of row crops (see fig. 2) replaced by the cover properties of bare clay with a Manning's *n* of 0.10, K_t of 0.10, K_d of 0.00089, and a τ_c of 0.01. Distributed rainfall infiltration as in table 1 for the CNII-D antecedent and soil conditions was applied but with an infiltration of 94 for the bare clay. Module *r.terradyn* was run for 15 iterations (~1 year) to model the duration of an extended construction project in the disturbed areas. The results of this simulation are presented in figure 6. Erosion was predicted for the disturbed areas with significant deposition along the

boundaries. Deposition within the channels was confined upstream from the watershed outlet due to the buffer land cover (grass-meadow). Vegetation within these areas of deposition would be threatened by the accumulation of sediment.

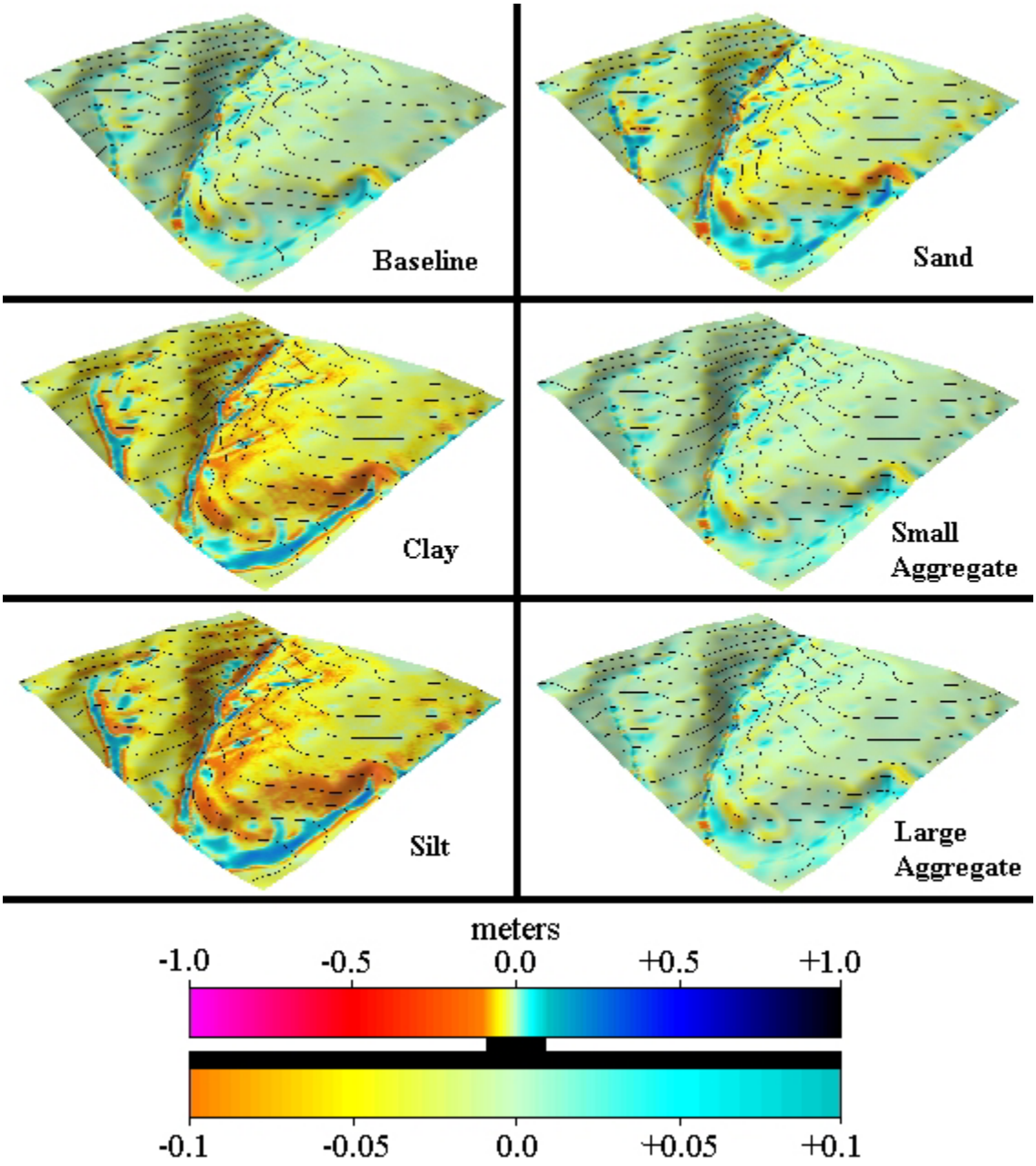

Figure 5: The modified DEM of the Lake Wheeler sub-watershed after 30 r.terradyn iterations for the baseline and for the 5 soil types (table 2) in which K_t=0.1, K_d =0.00089, and τ_c=0.01 (clay), K_t=0.02, K_d =0.00148, and τ_c=0.05 (silt), K_t=0.005, K_d =0.00155, and τ_c=0.1 (sand), K_t=0.0005, K_d =0.0110, and τ_c=0.8 (small aggregates), and K_t=0.0004, K_d =0.0128, and τ_c=1.0 (large aggregates).

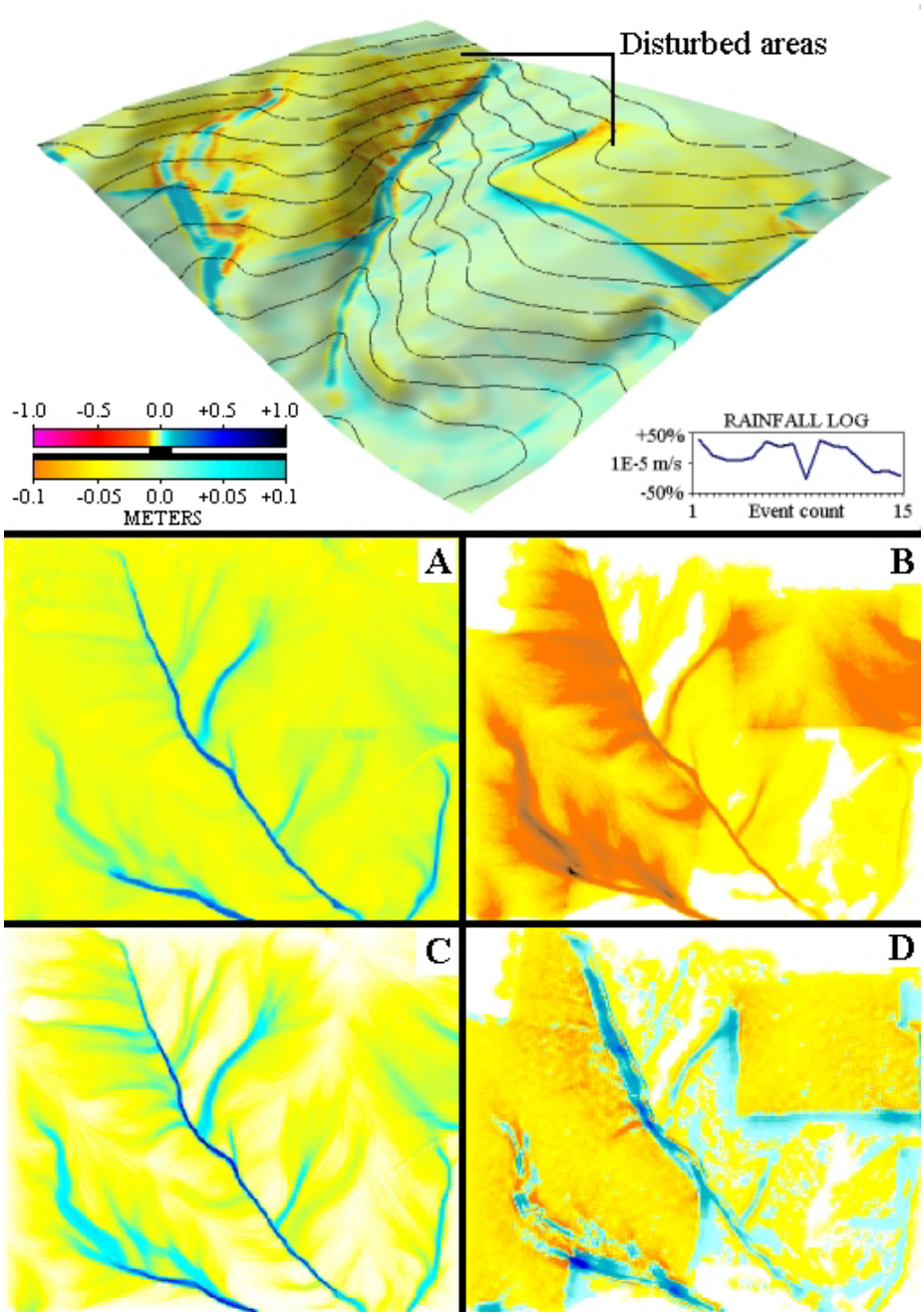

Figure 6: The modified DEM of the Lake Wheeler sub-watershed after 30 r.terradyn iterations with K_t=0.1 and K_d =2.2 (small aggregates). Also included are the (A) water depth [m], (B) sediment flux [kg/m/s], (C) flow discharge [m^3/s], and (D) erosion / deposition pattern (smoothed) [kg/m^2/s] from r.sim.sediment (not used by r.terradyn) at iteration #12, in which the rainfall was 1.3E-5 m/s.

Discussion and Conclusions

Due to the shallow hill slopes and the existence of substantial, static land cover throughout the watershed, elevation changes at the Lake Wheeler Road site in general have been minimal over the span of the last 2 years. This is consistent with the small terrain changes modeled as seen

for the baseline runs and for the distributed land cover and rainfall infiltration runs. In general, primary terrain change took the form of erosion of steeper slopes and channel banks, as well as deposition in areas of reduced transport capacity. During the evolution of the terrain, channels braided and meandered and rills were either incised or filled in, depending on the intensity of the individual rainfall events. Less terrain change was modeled for drier antecedent conditions (CNI) and for the type A soils, as well as for simulations employing distributed land cover. Higher rainfall rates were employed in the distributed land cover simulations to illustrate the potentially damaging sediment deposition in areas of lower transport capacity such as wooded areas. This effect was also obtained from simulations in which disturbed areas of bare clay were included in the study region.

Bare soil simulations used for grain size comparison demonstrated with reasonable skill the relative behaviors of grain size dependent erosion and deposition normally observed in the field. Small grains, transported under detachment-limited conditions, were detached but did not redeposit without significant reductions in transport capacity as seen in the channels and other areas of upward topographical convexity. Larger grains, transported under transport-limited conditions, detached and were transported small distances such that the terrain evolved with higher spatial variation in the erosion / deposition patterns relative to the small grain size runs. In addition, the grain size dependent simulation results showed that sediment erosion and deposition and terrain evolution was weakly sensitive to changes in the critical shear stress ranging from 0.01 to 1.00 - the magnitude of sensitivity toward this range in critical shear was on the same scale as variations in soil erosion and deposition and terrain evolution that arose due to the randomization of the input rainfall rates.

In this version of *r.terradyn*, terrain change stability was highly sensitive to the channel morphology. Without the band-pass filter, channel incision artificially dominated under all land cover conditions presented here - important small scale effects on the hillslopes became difficult to discern due to the processing necessary to visualize the results. Ideally, the band-pass filter would not be necessary. Alternatively, SIMWE as currently defined could be modified such that the shear stress is based on the depth of the effective boundary layer - not the total flow depth. A maximum allowable flow depth, possibly scaled by flow velocity, could be imposed upon the algorithm for calculating shear stress. These or similar corrections would desensitize SIMWE to channel (deeper water) flows and permit *r.terradyn* to function without concern for exponential channel incision or the need for the band-pass filter designed to attenuate this effect.

References

Borah, D.K. and M. Bera. 2003. Watershed-scale hydrologic and nonpoint-source pollution models: review of mathematical bases, Transactions of the ASAE 46(6): 1553-1566

Dabney, S.M. 1999. Lanscape Benching from Tillage Erosion Between Grass Hedges. Proceedings from ISCO Conference, CDROM, Lafayette: Purdue University.

Dietrich, W.E., C. J. Wilson, D. R. Montgomery, and J. McKean. 1993. Analysis of erosion thresholds, channel networks, and landscape morphology using a digital terrain model, Journal of Geology, 101(1), 259-278

Favis-Mortlock D., Boardman J., Parsons, T., Lascelles, B. 1998. Emergence and erosion: a model for rill initiation and development. Proceedings of the 3rd conference on GeoComputation (CDROM), University of Bristol, UK.

Foster, G.R. 1982. Modeling the Erosion Process, from Hydrologic Modeling of Small Watershed, ed. by C.T. Haan, H.P. Johnson, D.L. Brakensiek, ASAE

Foster, G.R., L.J. Lane, M.A. Nearing, S.C. Finkner, and D.C. Flanagan. 1989. USDA-Water Erosion Prediction Project (WEPP), Hillslope Profile Model Documentation, Chapter 10,

Erosion Component, NSERL Report No. 2, USDA-ARS National Soil Erosion Research Laboratory, West Lafayette, IN

Foster, G.R., D.C. Yoder, G.A. Weesies, and T.J. Toy. 2001. The design philosophy behind RUSLE2: evolution of an empirical model, pp. 95-98 in Soil Erosion Research for the 21st Century, Proc. Int. Symp. (3-5 January 2001, Honolulu, HI, USA). Eds. J.C. Ascough II and D.C. Flanagan. St. Joseph, MI: ASAE. 701P0007.

Haan, C.T., B.J. Barfield, and J.C. Hayes. 1994. Design Hydrology and Sedimentology for Small Catchments. San Diego, California: Academic Press

Horn, B.K.P. 1981. Hill shading and the reflectance map, Proceedings of the IEEE, 69(1), 14-47.

Karrambas, T.V. and C. Koutitas. 2002. Surf and swash zone morphology evolution induced by nonlinear waves, Journal of Waterway, Port, Coastal and Ocean Engineering, 128(3), 102-113.

Lei, T., M.A. Nearing, K. Haghighi, and D.A. Bulgakov. 1997. A model of soil erosion in a rill: Temporal evolution and spatial variability, ASAE Paper No. 973068, ASAE Annual International Summer Meeting, ASAE, St. Joseph, MI: ASAE

Mitas, L. and H. Mitasova. 1998. Distributed soil erosion simulation for effective erosion prevention, Water Resources Research, 34(3), pp. 505-516, March

Mitasova, H., J. Hofierka, M., Zlocha, and L.R. Iverson. 1996. Modeling topographic potential for erosion and deposition using GIS, International Journal of Geographical Information Systems 10(5): 629-641

Neteler, M. and H. Mitasova. 2002. Open source GIS: A GRASS GIS approach, Kluwer Academic Publishers, Boston, MA

Parker, G., C. Paola, S. Leclair, 2000, Probabilistic exner sediment continuity equation for mixtures with no active layer, Journal of Hydraulic Engineering, 126(11), 818-826

Renard, K.G., G.R. Foster, G.A. Weesies, D.K. McCool, and D.C. Yoder. 1997. Predicting soil erosion by water: a guide to conservation planning with the revised universal soil loss equation RUSLE, USDA, Agric. Handbook No. 703, pp. 404, U.S. Department of Agriculture, Washington, D.C.

Thaxton, C.S. 2004. Investigations of grain size dependent sediment transport phenomena on multiple scales, PhD dissertation, NC State University, Dept. of Physics, http://etd.ncsu.edu/

Tucker, G., S. Lancaster, N. Gasparini, and R. Bras. 2001. The channel-hillslope integrated landscape development model (CHILD), in Landscape erosion and evolution modeling, edited by R. S. Harmon and W. W. Doe III, pp. 349-388, Kluwer Academic/Plenum Publishers, New York.

Tucker, G.E. and R.L. Bras. 1998. Hillslope processes, drainage density, and landscape morphology, Water Resources Research 34(10): 2751-2764

Willgoose, G., R.L. Bras, and I. Rodriguez-Iturbe. 1991. A coupled channel network growth and hillslope evolution model 1. Theory, Water Resources Research, 27(7), 1671-1684

Wischmeier, W.H. and D.D. Smith. 1965. Predicting rainfall-erosion losses from cropland east of the Rocky Mountains-A guide for selection of practices for soil and water conservation, Agricultural Handbook No. 282. U.S. Department if Agriculture, Washington, D.C.

Wischmeier, W.H. and D.D. Smith. 1978. Predicting rainfall erosion losses -A guide to conservation planning, Agricultural Handbook No. 537. U.S. Department if Agriculture, Washington, D.C.

Young, R.A. and C.A.Onstad. 1978. Characterization of rill and interrill eroded soil, Transactions of the ASAE 21(6): 1126-1130